RSC Advances

ROYAL SOCIETY OF CHEMISTRY

www.rsc.org/advances

Synthesis of Graphene-like g-C_3N_4 / Fe_3O_4 Nanocomposites with High Photocatalytic Activity and for Drug Delivery

C. G. Liu[*a] , X. T. Wu[a], X. F. Li[b], X. G. Zhang[a]

a. Roll Forging Research Institute of Jilin University, Jilin University, Changchun, 130022, China

b. Key Laboratory of Functional Materials Physics and Chemistry of the Ministry of Education, Jilin Normal University, Siping 136000, Jilin, China

Abstract

Graphene-like g-C_3N_4 nanosheets (GCN) / Fe_3O_4 Quantum dot (QDs) nanocomposites were successfully synthesized by a facile electrostatic self-assembly method. Characterization shows that the GCN is at least several micrometers in size. The GCN/Fe_3O_4 nanocomposites were used as photocatalysts for degradation of Rhodamine B (RhB) under visible light irradiation, after irradiation for 1.5 h, the degradation efficiency was 72.5% for pure g-C_3N_4, 81% for GCN-1wt%Fe_3O_4, 95% for GCN-2wt%Fe_3O_4, 60.46% for GCN-3wt%Fe_3O_4 and 57.2% for GCN-4wt%Fe_3O_4, indicating that GCN-2wt% Fe_3O_4 nanocomposites had the highest photocatalytic activity. We deduce that the efficient separation of the photogenerated electron-hole pairs and the high specific surface area of GCN play important roles in the photocatalytic activity of the nanocomposites. In addition, the nanocomposites can loaded with model drug (Rhodamine B) and the loading capacity was as high as 108.6 $mg \cdot g^{-1}$, which making it a potential candidate for photocatalysis and controlled magnetic targeted drug delivery.

Keywords: graphene-like g-C_3N_4 nanosheets**,** Fe_3O_4 Quantum dot, photocatalysis, drug delivery.

[*] Corresponding author E-mail:wuxt12@mails.jlu.edu.cn. Tel: +86043185094340

1. Introduction

Graphite-like carbon nitride (g-C_3N_4), a novel metal-free direct bandgap semiconductor with bandgap of ca. 2.7 eV, has attracted intensive interest for its promising applications in photocatalysis, electrocatalysis, bioimaging and biomedical, etc[1-5]. A large amount of literatures have reported its ability of organic dyes degradation and hydrogen or oxygen production from water splitting under visible light irradiation[6.7], and more potential properties of g-C_3N_4 are improving rapidly[3,8-10].

Recently, much of research on ultrathin sheet-like nanostructure[11-14] has been conducted since the discovery of graphene (GR) which presents many unique and inspiring properties different from bulk graphite. In particular, GR-semiconductor nanocomposites show excellent performance in photocatalysis, and GR-magnetic nanoparticles (NPs) composite materials show the outstanding properties in drug delivery and biosensing[15.16]. So, motivated by such unique nature of graphene for its ultrathin sheet-like nanostructure, researchers have tried to synthesis the graphene-like g-C_3N_4 to obtain similar properties and application of graphene[17.18].

Different from graphite, the g-C_3N_4 layer is composed of C-N bonds instead of C-C bonds, and there is weak vander Waals force between the layers. Many groups tried to synthesis graphene-like ultrathin g-C_3N_4 nanosheets recently. Based on the experience of graphene, Liu et al. tried to exfoliate bulk g-C_3N_4 by the Hummers method which is widely used in graphene but failed[17]. It is attributed to the weaker hydrogen bonding between the layers of strands of polymeric melon units in g-C_3N_4, which is different from the planar pure covalent bonding cohesion within the graphite[19]. On this basis, the reaserchers successfully synthesized GCN via many other methods, Liu et al developed a direct thermal oxidation “etching” process of bulk g-C_3N_4 to get ultrathin g-C_3N_4 nanosheets[17], Zhu et al. prepared g-C_3N_4 nanosheets with a single atomic layer structure by a simple chemical exfoliation method[20], Wang et al. obtained ultrathin C_3N_4 nanosheets using a “bottom-up” method[21]. Ultrathin g-C_3N_4 nanosheets were also successfully prepared by

ultrasound exfoliation or liquid exfoliation method from bulk g-C_3N_4[18,22]. Furthermore, the more synthetic techniques for GCN vis-à-vis graphene including recently developed laser exfoliation[23] and laser reduction technique[24-26] should be developed and explored in our future work.

Although graphene-like g-C_3N_4 nanostructure has already can be obtained, few studies has been focused on the composite materials which are composed of graphene-like g-C_3N_4 nanosheets and magnetic nanoparticles (NPs), and the excellent properties of the graphene series composites in drug delivery and photocatalysis.

In the present work, we synthesized graphene-like ultrathin g-C_3N_4 nanosheets by ultrasound exfoliation method from bulk g-C_3N_4, and then prepared graphene-like g-C_3N_4 nanosheets/Fe_3O_4 quantum dot nanocomposites for the first time via an easy electrostatic self-assembly method, and their structural properties were systematically characterized. The effect of the amount of Fe_3O_4 contents in the g-C_3N_4 nanosheets/Fe_3O_4 nanocomposites on the photocatalytic activity under visible light irradiation was investigated. Moreover, we also conducted a pilot study on the drug loading capacity of the material.

2. Experimental

2.1 Preparation.

Preparation of graphene-like g-C_3N_4 nanosheets (GCN).

Briefly,10 g urea (A.R., Sinopharm Chemical Reagent Co.,Ltd) was dissolved in 20 ml deionized water under stirring for 15 min at room temperature, then the solution was put into an alumina crucible, and heated to 550℃ in tube furnace for 2 h. The synthetic yellow powder was collected for use. Finally, the as-prepared g-C_3N_4 was sonicated and washed with deionized water several times to get graphene-like ultrathin g-C_3N_4 nanosheets. Finally, the sample was dried at 60 ℃ for 24 h.

Preparation of Fe_3O_4 QDs.

Firstly, dissolved $FeCl_2 \cdot 4H_2O$ (A.R., Sinopharm Chemical Reagent Co.,Ltd) and $FeCl_3 \cdot 6H_2O$ (A.R., Sinopharm Chemical Reagent Co.,Ltd) with 1:2 molar ratios into deionized water, and stirred the mixed solution for 5 min. Then, added $NH_3 \cdot H_2O$

aqueous solution (25%, A.R., Sinopharm Chemical Reagent Co.,Ltd) into the above solution at 60 °C drop by drop. Waiting until the color of the solution changed from dark orange to black about 40 min later, which indicating the formation of Fe_3O_4 QDs. The as-prepared Fe_3O_4 QDs were magnetic separated and washed with deionized water and ethanol several times, and then dried in vacuum at 60 °C for 24 h.

Preparation of GCN/Fe_3O_4 **nanocomposites.**

GCN/Fe_3O_4 nanocomposites were prepared by the electrostatic self-assembly method : 100 mg GCN were dispersed in 50 ml of deionized water by ultrasound for 30 min. Meanwhile, different amounts (1 mg, 2 mg, 3 mg and 4 mg) Fe_3O_4 QDs were added into 10 ml of deionized water by ultrasound for 15 min. Then, added the suspension of Fe_3O_4 QDs to the suspension of GCN drop by drop under vigorous stirring. After that, the obtained mixed suspension was sealed and stirred for 24 h. Finally, the product was dried at 60 °C for 24h in a vacuum drying oven and then annealed at 150 °C in the vacuum drying oven for 2 h.

2.2 Characterization.

The characterizations of the samples were carried out via X-ray diffraction (XRD) patterns collected on MAC Science MXP-18 X-ray diffractometer using a Cu target radiation source; field-emission transmission electron microscope (FETEM) was performed on a JEOL JEM-2100F; Fourier transform infrared (FTIR) spectroscopy was recorded on a Bruker Vertex 70 spectrophotometer in KBr pellets; X-ray photoelectron spectrum measurement was performed on a Vgescalab MK II X-ray photoelectron spectrometer (XPS) using Mg Kα radiation (hν =1253.6 eV) with a resolution of 1.0 eV. The UV-Vis diffuse reflectance spectra (UV-Vis DRS) were obtained for the dry-pressed disk samples using Specord 2450 spectrometer (UV-3100) equipped with the integrated sphere accessory for diffuse reflectance spectra, using $BaSO_4$ as the reflectance sample. The surface areas of samples were measured by TriStar 3000-BET/BJH Surface Area.

2.3 Photocatalytic reaction

The photocatalytic degradation of rhodamine B (RhB) was carried out at room

temperature in a 250 mL glassy reactor containing catalyst (60 mg) and RhB aqueous solution (60 mL, 7 mg/L). Before photocatalytic reaction the catalyst were electric stirred thoroughly in the dark for reaching the adsorption equilibrium. The catalyst exposure to visible light using a 350W Xe lamp with cutoff 420 nm. After different irradiation intervals, the solution concentration of RhB was analyzed by a UV–vis spectrophotometer (UV-3100) at room temperature.

2.4 Conjugation of GCN/Fe_3O_4- RhB

Firstly, 10 mg GCN/Fe_3O_4 nanocomposites were added into the RhB solution with desired concentration, sonicated for 30 min and then stirred 24h at room temperature in the dark. After that, all solutions were ultracentrifuged at 14000 rpm for 20 min, the RhB concentration in the upper layer was measured via a standard RhB concentration curve generated by the UV- vis spectrophotometer from a series of RhB solutions with different concentrations. The amount of RB loaded on the GCN/Fe_3O_4 (Φ) was determined using the equation as follow: $\Phi = (M_{RhB} - M_{RhB'})/M_{GCN/Fe3O4}$, M_{RhB} is the initial amount of RhB, $M_{RhB'}$ is the amount of RhB in the upper layer, and $M_{GCN/Fe3O4}$ is the amount of the nanocomposites added.

3. Results and discussion

The XRD patterns of pure g-C_3N_4 and GCN/Fe_3O_4 nanocomposites are shown in Fig.1. We can found a strong peak at about 27.3° in all samples which represents the stacking of the conjugated aromatic system. It is indexed for the (002) peak of g-C_3N_4, which is corresponding to the interlayer d-spacing of 0.336 nm. The small peak in all samples at 12.9°, is indexed as (100) plane of g-C_3N_4, which is associated with interlayer stacking[27]. Fe_3O_4 characteristic peaks can be observed in nanocomposites which can be indexed as the pure facecentered cubic structure of Fe_3O_4 according to JCPDS card No.19-0629 [28], the low intensity of the peaks is due to the low amount of Fe_3O_4. These results indicate that the nanocomposites are composed of both g-C_3N_4 and Fe_3O_4. Then, the little difference of the g-C_3N_4 peaks between pure g-C_3N_4 and the nanocomposites suggests that the presence of Fe_3O_4 does not influence the crystal nature of g-C_3N_4 which is advantageous for the photocatalytic activity of the nanocomposites.

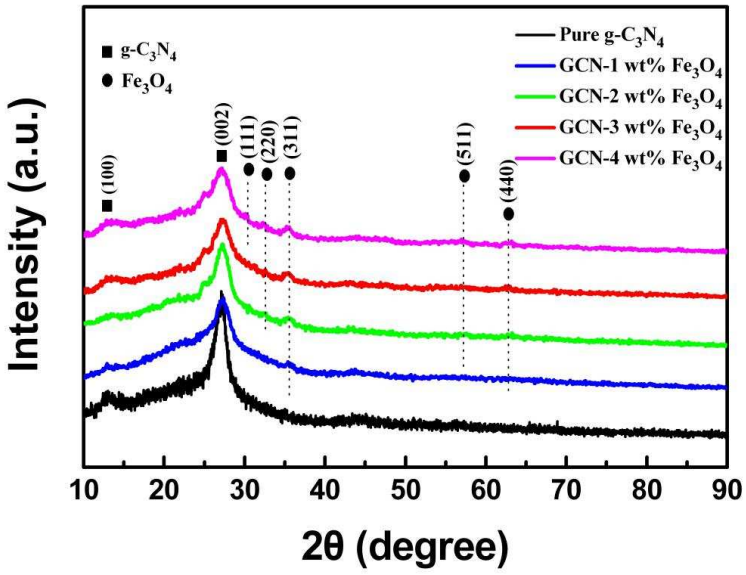

Fig.1 XRD patterns of pure g-C_3N_4 and GCN/Fe_3O_4 nanocomposites.

The typical TEM and HRTEM images of the GCN/Fe_3O_4 nanocomposites are shown in Fig.2. The thin silk-like structure of the graphene-like g-C_3N_4 nanosheets can be clearly observed in Fig. 2a, The lateral size of the transparent sheets are as large as several micrometers. The darker part in the image is the wrinkle or overlap of GCN. Fig. 2b shows the enlarge image of the nanocomposites. From Fig. 2b, the Fe_3O_4 QDs dispersed on the surface of the GCN were found, which had agglomeration to some extent. The HRTEM image of the composites are shown in Fig. 2c, the diameter of Fe_3O_4 QDs is about 10 nm, and we can found the lattice of Fe_3O_4 with the *d* spacing of about 0.297nm and 0.258nm, which are conforms to the (220) and (311) plane of face centered cubic Fe_3O_4[28]. The image also exhibit the intimate interfacial contact between GCN and Fe_3O_4 QDs. As the interfacial interaction have a great impact on the transfer process of charge carriers in the nanocomposites, it could be expected that there would be a good charge transfer during the photocatalysis process. All these results above show that the as-prepared sample is composited of two separate phases of Fe_3O_4 QDs and GCN.

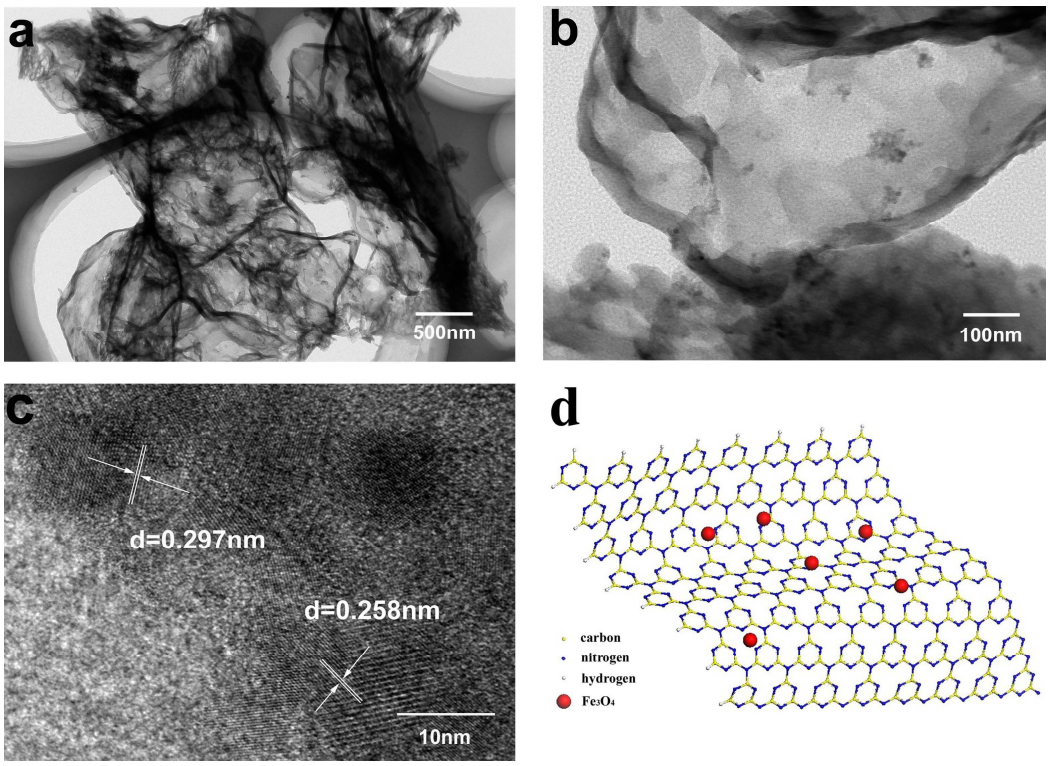

Fig. 2a and b TEM images of GCN/Fe_3O_4 nanocomposites; Fig. 2c HRTEM images of Fe_3O_4 QDs; Fig. 2d Models of GCN/Fe_3O_4 nanocomposites.

The absorption range of light is very important in the visible light photodegradation of contaminants, therefore, the UV-Vis diffuse reflectance spectra was measured and shows in Fig.3a. As a comparison, the spectrum of pure g-C_3N_4 was also measured. As the Fig.5a indicates, both two spectra have the broad absorption in the UV-visible region, which demonstrates that g-C_3N_4 and the nanocomposites possess visible-light absorption ability. Then, an obvious red shift in the absorption edge and enhanced absorption intensity of GCN/Fe_3O_4 samples were observed. This phenomenon maybe attributed to a charge-transfer transition between the Fe_3O_4 species and the g-C_3N_4 conduction or valence band, which can leading to stronger redox ability and higher photocatalytic activity[29].

The bond structure of GCN/Fe_3O_4 nanocomposites was studied by FTIR spectroscopy, as a comparison, the spectrum of pure g-C_3N_4 was also measured. The result is shown in Fig.3b: It can be seen several main characteristic peaks in both two

spectra, the peak at 809 cm^{-1} was related to the tri-s-triazine ring modes, several strong bands in the 1200-1650 cm^{-1} region correspond to the typical stretching modes of CN heterocycles; the peaks at 1635, 1569 and 1411 cm^{-1} were attributed to stretching vibration modes of heptazine-derived repeating units, which accord with the XRD result of pure g-C_3N_4. Then, the peaks at 1316 and 1238 cm^{-1} assigned to stretching vibration of connected trigonal units of C-N(-C)-C or bridging C-NH-C (partial condensation) [30]. In addition, the wide band between 3000-4000 cm^{-1} can be assigned to the absorption water or O-H groups. For GCN/Fe_3O_4 nanocomposites, the characteristic absorption of the Fe_3O_4 centered at 585 cm^{-1} was observed, which is corresponding to the vibration of the Fe-O bonds [31.32]. It can be clearly seen that all of the main characteristic peaks of g-C_3N_4 and Fe_3O_4 appeared in the Fe_3O_4/GCN, and there is no obvious peak shift between pure g-C_3N_4 and GCN/Fe_3O_4 nanocomposites. The intensity of the peaks has some variations compared with the pure g-C_3N_4, indicating that there are close interfacial connections between g-C_3N_4 and Fe_3O_4 rather than a simply physical adsorption [33], which is consistent with HRTEM results, and this connection may serve as electron migration paths to promote the charge separation, and leading to an improved photoactivity [34].

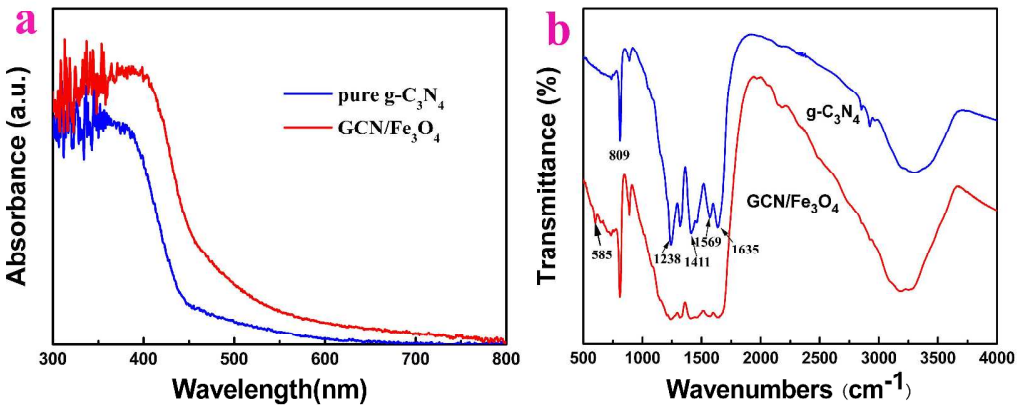

Fig. 3 Optical measurement of pure g-C_3N_4 and GCN/Fe_3O_4 nanocomposites (Fig. 3a UV-Vis diffuse reflectance spectra; Fig. 3b FTIR spectra).

The XPS spectrum analysis was employed to investigate the valence states and

chemical environment of constituent elements on the surface of GCN/Fe_3O_4 nanocomposites which is shown in Fig.4. Fig.4a shows survey spectra of the GCN/Fe_3O_4. O, C, N and Fe elements were detected in the nanocomposites. Fig. 5b shows the regional spectrum of C1s which can be deconvoluted into three peaks at 284.1, 286.8 and 287.8 eV, respectively. The peak at 284.6 eV is arising from the adventitious carbon, the peak at 286.1eV can be assigned to C–N-C coordination, then, another peak at 288eV can be attribute to the C-$(N)^3$ group of g-C_3N_4 [35-38]. The N1s region can be fitted into three peaks(Fig.4c), ascribabing to C–N–C (398.4eV), N–$(C)_3$ (400.1eV) and C–N–H groups (401.3eV), respectively [39]. The XPS data also gives an evidence for the existence of graphite-like sp^2-bonded structure in GCN. The Fe 2p region of the spectrum is shown in Fig.4d, two strong peaks centered at about 725and 711 eV, which respectively assigned to Fe 2p1/2 and Fe 2p3/2 for Fe_3O_4 [40.41] were observed. It is almost equalled to the standard binding energy of Fe_3O_4, suggesting Fe element exists as a Fe_3O_4 form in the nanocomposite [42]. Moreover, neither the peak of Fe-C or Fe-N was detected in the spectra, indicating that no chemical bond forming between Fe_3O_4 quantum dot and GCN, which is consistent with above study.

The At.% of every elements by calculating the peak areas , which are shown in Table 1:

Table 1 The At.% of every elements

Name	Peak BE	Height Counts	FWHM eV	Area (N)	At. %
C1s	284.6	12074.45	1.42	0.37	38.36
N1s	398.43	15284.8	1.39	0.45	47.74
O1s	532.54	8411.49	2.55	0.18	12.88
Fe2p	710.83	938.6	0.85	0	0.25

According to Table 1, the N:C ratio is 1.22, which is lower than the theoretical value (1.33). It may be mainly due to the structure defect result from the existence of chemica oxygenic functional groups like C=O, -COOH, amounts of oxygen may come from above groups and H_2O which is adsorbed to the surface of the sample.

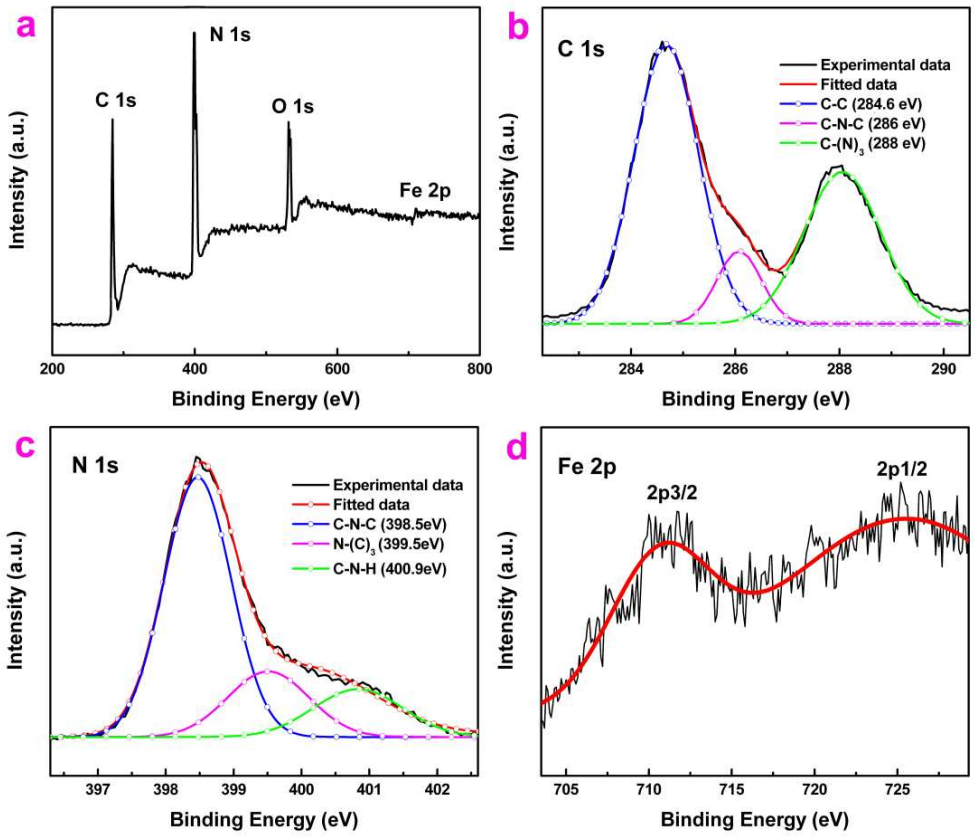

Fig. 4a XPS survey spectrum of GCN/Fe_3O_4 nanocomposites; Fig. 4b,c and d High-resolution binding energy spectrum of C 1s, N 1s, Fe 2p for the nanocomposites, respectively.

The photocatalytic activity of GCN/Fe_3O_4 nanocomposites with different loading amounts of Fe_3O_4 and pure g-C_3N_4 was evaluated by degrading the well-known organic dye RhB under visible-light irradiation. To fully consider the high adsorption ability of g-C_3N_4, adsorption equilibrium experiment also be performed before the catalytic activity. The adsorption capacities are shown in the Fig. 5a, it can be observed that all samples can achieve the absorption equilibrium within 60 min in the dark, and almost 59-83 % RhB was adsorbed. Pure g-C_3N_4 exhibited the best adsorptivity, and the adsorptivity of GCN/Fe_3O_4 nanocomposites decreased with the increasing amounts of Fe_3O_4, which is due to the lower surface area of Fe_3O_4. The photodegradation process

of RhB which was recorded by the temporal evolution of the spectrum is shown in Fig.5b. In order to observe photocatalytic activity of samples more visually, the degradation efficiency of samples after irradiation for 1.5h is plotted as a histogram (Fig.5c). From Fig.5b and c, the degradation efficiency after irradiation for 1.5h is 72.5% for pure g-C_3N_4, 81% for GCN-1wt%Fe_3O_4, 95% for GCN-2wt%Fe_3O_4, 60.46% for GCN-3wt%Fe_3O_4 and 57.2% for GCN-4wt%Fe_3O_4 , it is obvious that the photocatalytic activity was enhanced gradually with the increasing proportion of Fe_3O_4 at first, and the GCN-1wt%Fe_3O_4 and GCN-2wt%Fe_3O_4 can degrade RhB by nearly 100% within 90 min and 120 min, respectively. The as-prepared GCN-2wt%Fe_3O_4 showed the highest photocatalytic activity. However, the photocatalytic activity of the nanocomposites decrease with the further increasing proportion of Fe_3O_4. Remarkably, GCN-3wt%Fe_3O_4 and GCN-4wt%Fe_3O_4 performed lower photocatalytic activity than pure g-C_3N_4.

The mechanism of the photocatalytic activity of the samples under visible-light irradiation is proposed as follows: Under visible light irradiation, GCN was excited to generate photo-generated electrons from HOMO to LUMO. Without the presence of other materials, electrons will undergo a quick transition back to the value bond owing to the instability of excited states. Then, with introducing of Fe_3O_4 QDs, the photogenerated e^- in GCN could easily transfer to Fe_3O_4 (CB) through their interfacial interaction beacause the energy level of the CB of GCN is higher than the Fermi level of Fe_3O_4, thus hinders the electron-hole recombination[43-45]. Therefore, the greatly enhanced photocatalytic activity can be attributed to the promoted electron-hole separation by the electron transfer process, in addition to the large surface area of GCN. GCN-2wt%Fe_3O_4 exhibited the best photocatalytic property, indicating that the adsorption capacities, photogenerated holes and electrons transfer reach the optimum. However, with further increasing proportion of Fe_3O_4, the excess Fe_3O_4 QDs which cover the active sites on the g-C_3N_4 surface and thereby reduce the efficiency of charge separation[46].

Renewable catalytic activity is also very important for a photocatalyst, so the

stability and durability of the GCN-2wt%Fe_3O_4 nanocomposites was further studied by a recycling test which is shown in Fig. 5d. There is no significant loss of activity after three cycles of the degradation reaction, which indicates the superior stability and durability of the nanocomposites.

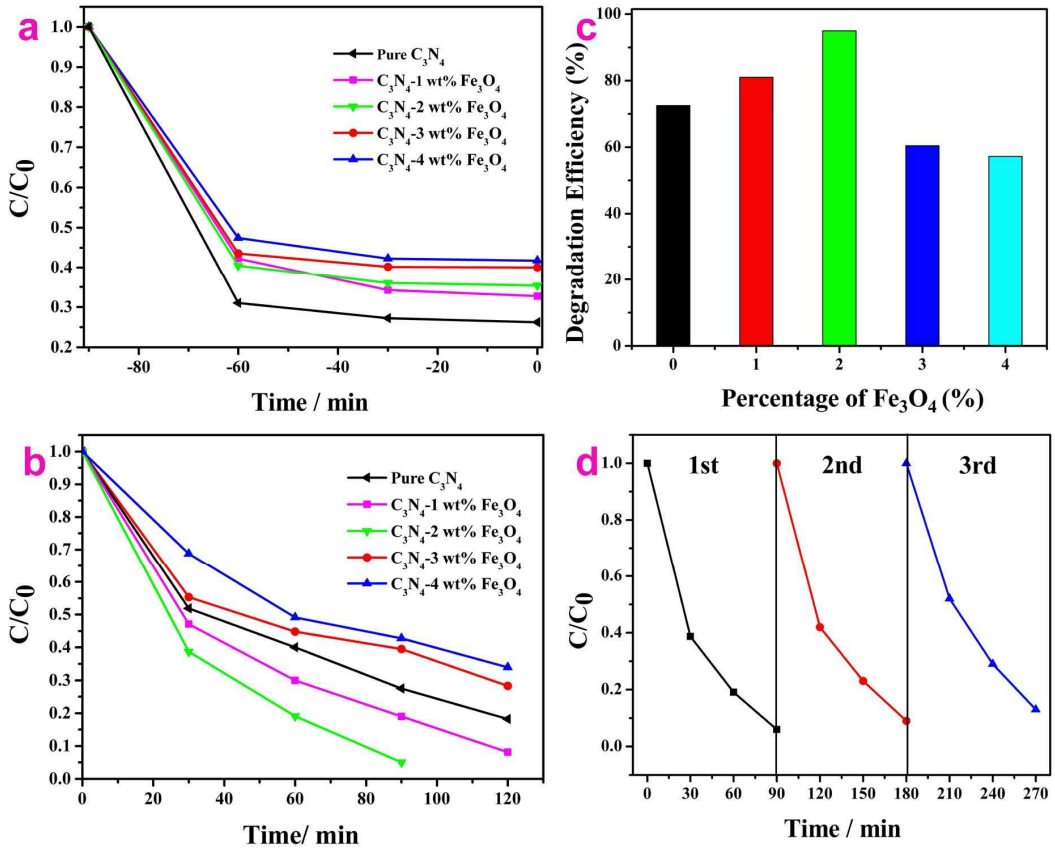

Fig. 5a The adsorption of pure g-C_3N_4 and GCN/Fe_3O_4 nanocomposites in the dark; b Photocatalytic degradation of RhB under the irradiation of visible light with pure g-C_3N_4 and GCN/Fe_3O_4 nanocomposites; c Degradation efficiency of pure g-C_3N_4 and GCN/Fe_3O_4 nanocomposites after irradiation for 1.5 h; d Reusability of the GCN-2wt%Fe_3O_4 nanocomposites in the visible light degradation of RhB.

The Brunauer Emmett Teller (BET) specific surface area and porous structure play an important role in drug load and delivery, so N_2 adsorption measurement was conducted. Fig.5a shows nitrogen adsorption-desorption isotherms and the corresponding pore size distribution curves of the GCN-2wt%Fe_3O_4 nanocomposites (inset in Fig.5a). From the adsorption isotherms, the BET specific surface area of the

sample was estimated to be 70 m^2/g. It has lower specific surface area than graphene (200 m^2/g), which is due to the stack of graphene-like sheets. The isotherms of the nanocomposites is type IV (Brunauer- Deming- Deming- Teller classification) and exhibit H_3 hysteresis loops which suggesting its sheet-like morphology and the slit-like mesopores [47], which is consistent with the TEM results (Fig. 2). As the inset shows, the pore-size distributions of the sample are very broad, indicating the existence of mesopores and macropores. For a high special external surface area, the nanocomposites may show large capacity of drug load and delivery.

To investigate loading capacity of the nanocomposites, we used the GCN-2wt%Fe_3O_4 nanocomposites to absorb RhB as a model drug determined by UV spectrum at 554 nm, which was calculated by the differences of RhB concentrations between the original RhB solution and the supernatant solution after loading. The saturated loading amount of RhB on the nanocomposites is shown in Fig.5b, which can reach 108 $mg \cdot g^{-1}$ at the RhB concentration of 20$mg \cdot L^{-1}$. Beside physical adsorption, hydrogen bonds, and electrostatic interaction [48] between GNSs and RhB may be also play important roles in loading. Therefore, in consideration of the loading capacity of GCN/Fe_3O_4 nanocomposites, it may be used as a potential candidate for controlled magnetic targeted drug delivery.

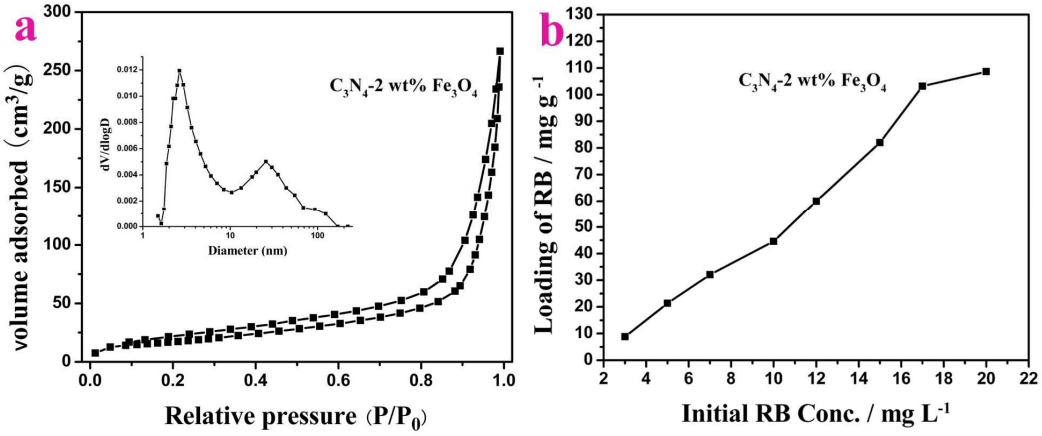

Fig. 6a Nitrogen adsorption-desorption isotherms and pore size distribution profiles of GCN-2wt%Fe_3O_4 nanocomposites; b Loading capacity of RhB on GCN-2wt%Fe_3O_4 nanocomposites in different initial RhB concentrations.

Conclusion

In this paper, we synthesized graphene-like ultrathin g-C_3N_4 nanosheets by ultrasound exfoliation method from bulk g-C_3N_4, and then graphene-like g-C_3N_4 nanosheets (GCN) / Fe_3O_4 Quantum dot (QDs) nanocomposites were obtained via electrostatic self-assembly method. The photocatalytic activity of GCN/Fe_3O_4 nanocomposites were evaluated under visible light irradiation, it has been seen that GCN-2wt% Fe_3O_4 nanocomposites had the highest photocatalytic activity. The mechanism of the highly enhanced photocatalytic property is attributed to the efficient separation of the photogenerated electron-hole pairs and the high specific surface area of graphene-like g-C_3N_4 nanosheets. Moreover, the nanocomposites can load model drug (Rhodamine B) and the loading capacity was as high as 108.6 $mg \cdot g^{-1}$, so the nanocomposites possess great potential applications in photocatalysis and controlled magnetic targeted drug delivery, perhaps even in many newly born properties for their enhanced intrinsic properties.

Acknowledgment

This work was supported by the National Programs for High Technology Research and Development of China (863) (Item No. 2013AA032202) and the National Youth Program Foundation of China (Grant Nos. 61308095)

References

[1] G. Liu, P. Niu, C. H. Sun, S. C. Smith, Z. G. Chen, G. Q. Lu and H. M. Cheng, *J. Am. Chem. Soc.*, 2010, **132**, 11642.

[2] X. Zhang, X. Xie, H. Wang, J. Zhang, B. Pan and Y. Xie, *J. Am. Chem. Soc.*, 2013, **135**, 18.

[3] Y. Zhang, A. Thomas, M. Antonietti and X. Wang, *J. Am. Chem. Soc.*, 2009, **131**, 50.

[4] Z. H. Zhang, K. Leinenweber, M. Bauer, L. A. J. Garvie, P. F. McMillan and G. H. Wolf, *J. Am. Chem. Soc.*, 2001, **123**, 7788.

[5] J. Sun, J. Zhang, M. Zhang, M. Antonietti, X. Fu and X. Wang, *Nat. Commun.*, 2012, **3**, 1139.

[6] X. C. Wang , K. Maeda , A. Thomas , K. Takanabe , G. Xin , J. M. Carlsson , K. Domen, M. Antonietti , Nat. Mater., 2009, **8**, 76.

[7] G. Liu, J.C. Yu, G.Q. Lu, H.M. Cheng, *Chem. Commun.,* 2011, **47,** 6763.

[8] Y. J. Cui, Z. X. Ding, X. Z. Fu and X. C. Wang, *Angew. Chem., Int. Ed.*, 2012, **51**, 11814.

[9] J. Liang, Y. Zheng, J. Chen, J. Liu, D. Hulicova-Jurcakova, M. Jaroniec and S. Z. Qiao, *Angew. Chem., Int. Ed.*, 2012, **51**, 3892.

[10] F. Z. Su, S. C. Mathew, L. Mohlmann, M. Antonietti, X. C. Wang and S. Blechert, *Angew. Chem., Int. Ed.*, 2011, **50**, 657.

[11] T. Brugger, H. F. Ma, M. Iannuzzi, S. Berner, A. Winkler, J. Hutter, J. Osterwalder and T. Greber, *Angew. Chem., Int. Ed.*, 2010, **49**, 6120.

[12] G. Eda, T. Fujita, H. Yamaguchi, D. Voiry, M. W. Chen and M. Chhowalla, *ACS Nano.*, 2012, **6**, 7311.

[13] S. Helveg, J. V. Lauritsen, E. Laegsgaard, I. Stensgaard, J. K. Norskov, B. S. Clausen, H. Topsoe and F. Besenbacher, *Phys. Rev. Lett.*, 2000, **84**, 951.

[14] J. Feng, L. Peng, C. Wu, X. Sun, S. Hu, C. Lin, J. Dai, J. Yang and Y. Xie, *Adv. Mater.*, 2012, **24**, 1917.

[15] X.F. Zhang, L. Clime, H.Q. Ly, M. Trudeau, T. Veres, *J. Phys. Chem. C*, 2010, **114**, 18313.

[16] X.Y. Li, X.L. Huang, D.P. Liu, X. Wang, S.Y. Song, L. Zhou and H.J. Zhang, *J. Phys. Chem. C*, 2011, **115**, 21567.

[17] P. Niu, L. Zhang, G. Liu and H.-M. Cheng, *Adv. Funct. Mater.*, 2012, **22**, 4763.

[18] S. Yang, Y. Gong, J. Zhang, L. Zhan, L. Ma, Z. Fang, R. Vajtai, X. Wang and P. M. Ajayan, *Adv. Mater.*, 2013, **25**, 2452.

[19] B. V. Lotsch, M. Doblinger, J. Sehnert, L. Seyfarth, J. Senker, O. Oeckler and W. Schnick, *Chem.–Eur. J.*, 2007, **13**, 4969.

[20] J. Xu, L.W. Zhang, R. Shi and Y. F. Zhu, *J. Mater. Chem. A*, 2013, **1**, 14766.

[21] Z. Lin and X. Wang, *Angew. Chem., Int. Ed.*, 2013, **52**, 1735.

[22] X. Zhang, X. Xie, H. Wang, J. Zhang, B. Pan and Y. Xie, *J. Am.Chem. Soc.*, 2013, **135**, 18.

[23] P. Kumar, *RSC Advances*, 2013, **3**, 11987.

[24] P. Kumar, B. Das, B. Chitara, K. S. Subrahmanyam, K. Gopalakrishnan, S. B. Krupanidhi, C.

N. R. Rao, *Macromolecular Chemistry and Physics*, 2012, **213**, 1146.

[25] P. Kumar, K. S. Subrahmanyam, C. N. R. Rao, *International Journal of Nanoscience*, 2011, **10**, 559.

[26] P. Kumar, K. S. Subrahmanyam, C. N. R. Rao, *Materials Express*, 2011, **1**, 252.

[27] L. Ge, *Mater. Lett.*, 2011, **65**, 2652.

[28] S.H. Xuan, F. Wang, J.M.Y. Lai, K.Y. Sham, Y.X.J. Wang, S.F. Lee, J.C. Yu, C.H.K. Cheng, K.C.F. Leung, *Appl. Mater. Interfaces*, 2011, **3**, 237.

[29] J. Xu, Y.J. Wang and Y.F. Zhu, *Langmuir*, 2013, **29**, 10566.

[30] J. H. Liu, T. K. Zhang, Z. C. Wang, G. Dawsona, W. Chen, *J. Materials Chemistry*, 2011, **10**, 1039.

[31] X. Yu, J. Wan, Y. Shan, K. Chen and X. Han, *Chem. Mater.*, 2009, **21**, 4892.

[32] M. Zhu and G. Diao, *J. Phys. Chem. C*, 2011, **115**, 18923.

[33] Y.J. Wang, Z.X. Wang, S. Muhammad, J. He, *Cryst. Eng. Comm.*, 2012, **10**, 1039.

[34] B. Chai, T.Y. Peng, J. Mao, K. Li and L. Zan, *Phys. Chem. Chem. Phys.*, 2012, **14**, 16745.

[35] J. H. Liu, T. K. Zhang, Z. C. Wang, G. Dawson and W. Chen, *J. Mater. Chem.*, 2011, **21**, 14398.

[36] F. Dong, L. W. Wu, Y. J. Sun, M. Fu, Z. B. Wu and S. C. Lee, *J. Mater. Chem.*, 2011, **21**, 15171.

[37] S. C. Yan, S. B. Lv, Z. S. Li and Z. G. Zou, *Dalton Trans.*, 2010, **39**, 1488.

[38] X. X. Xu, G. Liu, C. Randorn and J. T. S. Irvine, *Int. J. Hydrogen Energy*, 2011, **36**, 13501.

[39] Q.J. Xiang, J.G. Yu, M. Jaroniec, *J. Phys. Chem. C*, 2011, **115**, 7355.

[40] Y.J. Chen, G. Xiao, T.S. Wang, Q.Y. Ouyang, L.H. Qi, Y. Ma, P. Gao, C.L. Zhu, M.S.Cao, *J. Phys. Chem. C*, 2011, **115**, 13603.

[41] Z.S. Wu, S.B. Yang, Y. Sun, K. Parvez, X.L. Feng, K. Mullen, *J. American Society*, 2012, **134** 9082.

[42] J. S. Jang, S. H. Choi, H. G. Kim and J. S. Lee, *J. Phys. Chem. C*, 2008, **112**, 17200.

[43] N. Li, G. Liu, C. Zhen, F. Li, L.L. Zhang, and H. M. Cheng, *Adv. Funct. Mater.,* 2011, **21**, 1717.

[44] K.F. Zhou, Y.H. Zhu, X.L. Yang, X. Jiang and C.Z. Li, *New J. Chem.,* 2011, **35,** 353.

[45] L. Gu, J.Y. Wang, Z.J. Zou, X.J. Han, *Journal of Hazardous Materials,* 2014, **268**,216.

[46] S. Ye, L. G. Qiu, Y. P. Yuan, Y.J. Zhu, J. Xia and J. F. Zhu, *J. Mater. Chem. A*, 2013, **1**, 3008.

[47] J. X. Sun, Y. P. Yuan, L. G. Qiu, X. Jiang, A. J. Xie, Y. H. Shen and J. F. Zhu, *Dalton Trans.*, 2012, **41**, 6756.

[48] R. Y. Zhang, M. Hummelgard, G. Lv, O. Hakan, *Carbon*, 2011, **49**, 1126.